Islanded Microgrid Voltage Control Structure Small-Signal Stability Analysis

Guy Wanlongo Ndiwulu and Emmanuel De Jaeger
IMMC/Mechatronic, Electrical Energy, and Dynamic Systems
Université catholique de Louvain (UCLouvain)
Louvain-la-Neuve, Belgium
{guy.wanlongo, emmanuel.dejaeger}@uclouvain.be

Angelo Kuti Lusala
Polytechnic Faculty, Department of electromechanics
Université Kongo (UK)
Kongo Central, Democratic Republic of the Congo
kutilusala@gmail.com

***Abstract*—Voltage and frequency stability is one major concern within inverter-based microgrid operating in islanded mode. Control of those interfaced inverters in grid-forming mode is one of the proper solutions, which has been widely discussed to improve the islanded microgrid stability. However, impacts of voltage control structure based on conventional proportional-integral controllers (PI) as suitable control technique, on islanded microgrid dynamics and stability, have not been distinctly investigated. Therefore, much control structures, with or without additional loops such as feedforward and decoupling loops, can be found in existing literature when the d-axis and q-axis synchronous reference frame is adopted. This paper proposes a thorough control structure analysis by considering the influence of each supplementary loop on inverter dynamics and stability, and on microgrid. System stability is investigated through computation and trajectory analysis of inverter small-signal model eigenvalues plotted in the complex plane. The obtained modelling results are compared with two model results reported in literature. These show that the effects of feedforward and decoupling loops strongly influence the microgrid dynamics and these help identify robust voltage control structure.**

***Index Terms*—Islanded microgrids, inverter, grid-forming control, small-signal stability.**

I. Introduction

An islanded microgrid can be considered as a low-voltage three-phase or single-phase local electric system with distributed energy generators, energy storage devices and loads, able to operate without connection to main grid. This electrical system technology is very different compared to conventional power systems. The main reason is that it depends on interfaced power converters based distributed sources for ensuring system integrity and stability. Hence, adequate control strategies are required and these are implemented into power converters, in order to ensure stable system operation of islanded microgrid among others. Power converters used in microgrids can be controlled in grid-forming mode [1]-[4]. This consists of an AC voltage source able to control the voltage amplitude and frequency of the islanded microgrid by using local measurements of current and voltage. This is often carried out using proportional-integral controllers (PI), in a two-loops control structure composed of external (outer) voltage loop and internal (inner) current control loop. The two loops present different bandwidth characteristics and they influence strongly the islanded microgrid dynamics and stability.

Grid forming control structure with PI controllers depends on the reference frame in which these controllers are implemented [4]. The dq-reference frame is often chosen because it results in a generally slower dynamics of the state variables. Zero control error is a general property of PI controllers, independent from the system, provided that these controllers are correctly designed and properly tuned [1], [4]. Although this brings advantages, one important concern of its application for islanded microgrid under grid-forming control mode is the impact on system dynamics and stability. Indeed one has to take care of the complexity introduced by additional decoupling and feedforward loops possibly present in the voltage control structure. These complexities make that control schemes based on PI controllers are implemented in various ways according to the authors [5]-[8]. However, no small-signal stability investigation to analyze influence of these additional loops on system dynamics and stability is systematically proposed in the literature.

This paper proposes a thorough control scheme analysis by considering impacts of the whole feedforward and decoupling loops on inverter dynamics and stability. To do this, the inverter small-signal model is developed in the dq-synchronous reference frame. The analysis is performed for a balanced three-phase system fed by a single three-phase voltage source inverter (VSI) with the associated control structure, LC filter and coupling impedance. The inverter stability is investigated through the computation of the eigenvalues and the analysis of the sensibility of each feedforward and decoupling loops on dominant poles in the complex plane. The obtained results are compared to the small-signal stability results of voltage control structures proposed in [5] and in [6]-[8]. Impacts of different loops on positioning the poles in the stable region are considered as comparison criterion. Finally, time domain simulation results

978-1-5386-4722-6/19/$31.00 ©2019 IEEE

are presented to demonstrate the impacts of each additional loops on the inverter dynamic performance.

The paper is organized as follows: section II presents the grid-forming control structure by giving its mathematical formulation and the observed differences among the references [5]-[8]. Section III compares the dynamic performance of the proposed approach and the approaches developed in [5]-[8]. Finally, section IV draws some conclusion.

II. Grid-Forming Control Approach

Fig. 1a describes the block diagram of the three-phase voltage source inverter (VSI) based distributed energy generator in which grid-forming control mode is implemented. The entire system consists of a power and a controller side as illustrated in Fig. 1b. The first one represents the AC microgrid at which the inverter is connected via LC filter and coupling impedance.

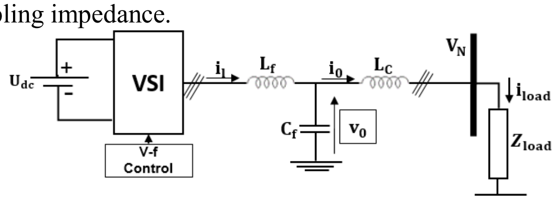

Fig. 1a. Single VSI supports one constant impedance load.

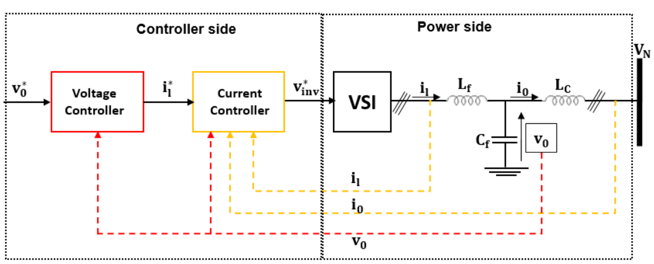

Fig. 1b. Block diagram of the voltage source inverter-based distributed generator and its control scheme in the three-phase grid-forming mode.

The controller side ensures regulation of the voltage magnitude and frequency to the power side. Frequency is maintained through the instantaneous phase angle that is used for each transformation between natural frame and rotating reference frame. Equation (1) shows that the dq-axis synchronous reference frame rotates with frequency ω whose rotating angle is equal to θ=ωt+δ. Phase angle δ (constant) is often zero for the inverter implemented in V-f control mode.

$$v_{0d} + jv_{0q} = \frac{2}{3}\left(v_{0a} + v_{0b}e^{\frac{j2\pi}{3}} + v_{0c}e^{-\frac{j2\pi}{3}}\right)e^{-j\theta} \qquad (1)$$

Voltage amplitude control is carried out by combining external voltage and internal current control loops in order to control both voltage magnitude and transient current due to the inrush currents within microgrid. The two control loops can be implemented by using the conventional PI controllers in dq-reference frame by including additional loops at the output of each control loops.

A. *Mathematical formulation*

Kirchhoff's voltage law application to the inverter power side in Fig. 1 are given in d-axis and q-axis rotating frame by equations (2) and (3). They include the LC filter dynamics constituted of L_f, C_f, i_{ld}, i_{lq}, v_{0d} and v_{0q}, and current of loads i_{0d} and i_{0q}.

$$\begin{bmatrix} v_{invd} \\ v_{invq} \end{bmatrix} - \begin{bmatrix} v_{0d} \\ v_{0q} \end{bmatrix} = L_f\frac{d}{dt}\begin{bmatrix} i_{ld} \\ i_{lq} \end{bmatrix} + R_f\begin{bmatrix} i_{ld} \\ i_{lq} \end{bmatrix} - \begin{bmatrix} 0 & \omega L_f \\ -\omega L_f & 0 \end{bmatrix}\begin{bmatrix} i_{ld} \\ i_{lq} \end{bmatrix} \qquad (2)$$

$$C_f\frac{d}{dt}\begin{bmatrix} v_{0d} \\ v_{0q} \end{bmatrix} - \begin{bmatrix} 0 & \omega C_f \\ -\omega C_f & 0 \end{bmatrix}\begin{bmatrix} v_{0d} \\ v_{0q} \end{bmatrix} = \begin{bmatrix} i_{ld} \\ i_{lq} \end{bmatrix} - \begin{bmatrix} i_{0d} \\ i_{0q} \end{bmatrix} \qquad (3)$$

Laplace's formulation in s-domain is given by

$$\begin{bmatrix} v_{invd}(s) \\ v_{invq}(s) \end{bmatrix} - \begin{bmatrix} v_{0d}(s) \\ v_{0q}(s) \end{bmatrix} = (sL_f + R_f)\begin{bmatrix} i_{ld}(s) \\ i_{lq}(s) \end{bmatrix} - \begin{bmatrix} 0 & \omega L_f \\ -\omega L_f & 0 \end{bmatrix}\begin{bmatrix} i_{ld}(s) \\ i_{lq}(s) \end{bmatrix} \qquad (4)$$

$$sC_f\begin{bmatrix} v_{0d}(s) \\ v_{0q}(s) \end{bmatrix} - \begin{bmatrix} 0 & \omega C_f \\ -\omega C_f & 0 \end{bmatrix}\begin{bmatrix} v_{0d}(s) \\ v_{0q}(s) \end{bmatrix} = \begin{bmatrix} i_{ld}(s) \\ i_{lq}(s) \end{bmatrix} - \begin{bmatrix} i_{0d}(s) \\ i_{0q}(s) \end{bmatrix} \qquad (5)$$

Where i_{0d} and i_{0q} are the direct and quadrature components of the current at the output of the filter. i_{ld} and i_{lq} are the direct and quadrature components of the current on the inductance of the filter. L_f and C_f are the inductance and capacitance of the LC filter. i_{cd} and i_{cq} can be defined as currents through the capacitance ($i_{cd(q)}=\omega C_f v_{0d(q)}$). $\omega L_f i_{ld}$ and $\omega L_f i_{lq}$ are the coupling terms provided by Park's transformation. v_{0d} and v_{0q} are the filter capacitance voltage.

The system's block diagram corresponding to the equations in the s-domain is depicted in Fig. 2. It is composed of four loops: feedback of v_0, coupling terms of current on filter inductance, current through the filter capacitance, and current load i_0 which has to be expressed, in the most general case, as a function $f(v_0)$ of the voltage at the output of the filter. Besides, this physical model shows that three of these loops depend on the filter, while i_0 represents the load and is related to the behavior of load in function of the voltage. It can be linked to the function $f(v_{0d},v_{0d})$ of v_0, then it can be considered as disturbances in the physical system.

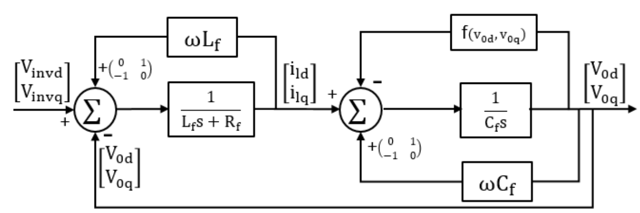

Fig. 2. Physical system obtained in the s-domain.

B. *The proposed voltage control structure compared to [5] and to [6]-[8]*

The proposed control scheme in d-axis and q-axis is given in Fig. 3. It consists of inner current and outer voltage control loops. The feedforward loops of $v_{0d(q)}$ and decoupling terms of $\omega L_f i_{ld(q)}$ are added at the output of the current control loop (indicated in green on Fig. 3) in order to compensate the opposite signals of physical feedback of $v_{0d(q)}$ and coupling terms through the filter current, respectively. The decoupling loops are a consequence of Park's transformation, while feedforward loops are inserted to compensate the LC filter dynamics. However, the reported investigation results in the existing literature show that some authors do not include these loops in their voltage control structures like in [5] and in [6]-[8]. [5] does not consider the decoupling loops. In [6]-[8], the feedforward loops of $v_{0d(q)}$ are neglected.

In addition, the current injection of loads $i_{0d(q)}$ in the physical system is balanced by inserting feedforward loops of $i_{0d(q)}$ at the output of the voltage control loop. The feedforward of current through the filter capacitor ($\omega C_f v_{0d(q)}$) is added at the same output loop (indicated in red on Fig. 3). Nevertheless, some references do not consider these loops [5].

The two above mentioned typical cases illustrate that several voltage control algorithms are found in the literature. Most of them neglect the decoupling and feedforward loops without investigating their influence on system dynamics and stability. Thus, this paper proposes a thorough analysis by considering impacts of the supplementary loops of the detailed control algorithm presented in Fig. 4 where all compensation and decoupling loops are included. Its dynamic performance is compared to the obtained results of the proposed control scheme of [5] and of [6]-[8].

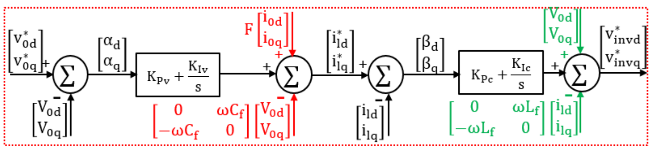

Fig. 3. Proposed voltage control structure in d-axis and q-axis synchronous reference frame.

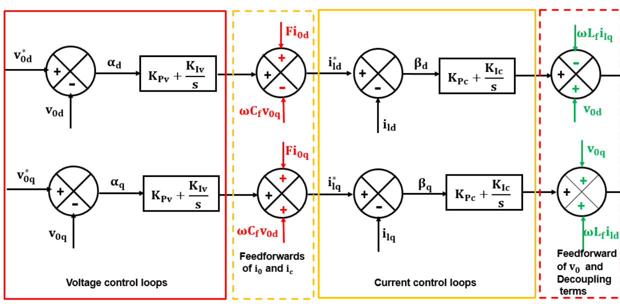

Fig. 4. Detailed voltage control structure in three-phase grid-forming voltage source inverter with compensation of i_0 , i_c , v_0 and coupling terms.

III. Stability Analysis Results

A. Small-signal model

The small-signal analysis is used as a tool to investigate the impact of additional loops on the system dynamic performance and stability. Hence, the state-space model of inverter according to its physical model depicted in Fig. 2 has to be established. It is composed of small-signal sub-models of voltage control loops, current control loops, LC filter and inductance coupling. The proposed description of each small-signal sub-model and the state-space inverter model are given by equations (6) to (8).

$$[\Delta x_{inv}] = \left[\Delta\alpha_{dq}\ \Delta\beta_{dq}\ \Delta i_{ldq}\ \Delta v_{0dq}\ \Delta i_{0dq}\right]^T \tag{6}$$

$$[\Delta \dot{x}_{inv}] = A_{inv}[\Delta x_{inv}] + B_{inv}[\Delta v_{NDQ}] \tag{7}$$

$$[\Delta i_{0DQ}] = C_{inv}[\Delta x_{inv}] \tag{8}$$

Equation (6) gives the state-space vector. Where, α_d and α_q are the output signal of the voltage comparator in d-axis and q-axis. β_d and β_q are the output signal of the current comparator. v_{ND} and v_{NQ} are the obtained input voltage of the controller in the D- and Q-axis common reference frame. i_{0D} and i_{0Q} are the output current of the inverter (i_0) injected to the microgrid transformed in the D-Q reference frame.

A_{inv} is the dynamic matrix, given by

$$A_{inv} = \begin{bmatrix} 0 & 0 & A_{v2} \\ F_{c1}C_v & 0 & F_{c1}E_{v2} + F_{c2} \\ B_{LCC1}G_{c1}C_v & B_{LCC1}C_C & A_{LCC} + B_{LCC1}(G_{c1}E_{v2} + G_{c2}) \end{bmatrix}_{10x10} \tag{9}$$

The controller parameters and LC filter factors characterize the proposed dynamic matrix. Its elements are the sub-matrices composed by controller gains and, inductance and capacitance of LC filter. They are given below where K_{Pv} and K_{Iv} are the proportional and integral gains of voltage control loop, respectively. K_{Pc} and K_{Ic} are the proportional and integral gains of current control loop. These controller gains (K_{Pv} , K_{Iv}, K_{Pc} and K_{Ic}) in each axis can be computed according to the analytical method developed in [10]. The cut-off frequency ω_n of the closed loop transfer function of the current control loop is set to ten times greater than for the external voltage control loops.

$$A_{v2} = \begin{bmatrix} 0 & 0 & -1 & 0 & 0 & 0 \\ 0 & 0 & 0 & -1 & 0 & 0 \end{bmatrix}\ C_v = \begin{bmatrix} K_{Iv} & 0 \\ 0 & K_{Iv} \end{bmatrix}\ C_C = \begin{bmatrix} K_{Ic} & 0 \\ 0 & K_{Ic} \end{bmatrix}$$

$$E_{v2} = \begin{bmatrix} 0 & 0 & -K_{Pv} & -\omega C_f & F & 0 \\ 0 & 0 & \omega C_f & -K_{Pv} & 0 & F \end{bmatrix}\ F_{c1} = \begin{bmatrix} 1 & 0 \\ 0 & 1 \end{bmatrix}\ G_{c1} = \begin{bmatrix} K_{Pc} & 0 \\ 0 & K_{Pc} \end{bmatrix}$$

$$G_{c2} = \begin{bmatrix} -K_{Pc} & -\omega L_f & 1 & 0 & 0 & 0 \\ \omega L_f & -K_{Pc} & 0 & 1 & 0 & 0 \end{bmatrix}\ F_{c2} = \begin{bmatrix} -1 & 0 & 0 & 0 & 0 & 0 \\ 0 & -1 & 0 & 0 & 0 & 0 \end{bmatrix}$$

$$A_{LCC} = \begin{bmatrix} -R_f/L_f & \omega & -1/L_f & 0 & 0 & 0 \\ -\omega & -R_f/L_f & 0 & -1/L_f & 0 & 0 \\ 1/C_f & 0 & 0 & \omega & -1/C_f & 0 \\ 0 & 1/C_f & -\omega & 0 & 0 & -1/C_f \\ 0 & 0 & 1/L_C & 0 & -R_C/L_C & \omega \\ 0 & 0 & 0 & 1/L_C & -\omega & -R_C/L_C \end{bmatrix}$$

$$B_{LCC1} = \begin{bmatrix} 0 & 1/L_f & 0 & 0 & 0 & 0 \\ 1/L_f & 0 & 0 & 0 & 0 & 0 \end{bmatrix}^T B_{LCL} = \begin{bmatrix} 0 & 0 & 0 & 0 & 0 & -R_C/L_C \\ 0 & 0 & 0 & 0 & -R_C/L_C & 0 \end{bmatrix}^T$$

B_{inv} is the input matrix. It is defined by voltage measurements at the connected inverter node. C_{inv} is the output matrix linked to the current injected by the inverter at the connected node. Equation (10) gives the two matrices with T_S define as the changing of reference frame matrix explained in [10]. Where B_{LCL} is a submatrix given above.

$$B_{inv} = [0\ \ 0\ \ B_{LCL}T_s^{-1}\ ]_{10x2}^T\ ;\ \ C_{inv} = [0\ \ 0\ \ 0\ \ \ \ 0\ \ T_s]_{2x10} \tag{10}$$

TABLE I. PARAMETERS VALUES OF THE SYSTEM COMPONENTS

Coupling impedance	Inductance : 0.35mH and Resistance: 0.03Ω
LC Filter	Inductance: 5mH ; Capacitance: 200µF ; f_{sw}=500Hz Resistance : 0.5Ω
RL load	400V ; 25kW ; 0.25kVAr ; v_{0dref}=320V ; v_{0qref}=0 cos**φ**=0.9
Controller	Inner loops : ω_{nIn}=4000rad/s; K_{Ic}=53e3 ; K_{Pc}=27 Outer loops: ω_{nEx}=400rad/s; K_{Iv}=390 ; K_{Pv}=0.14 Damping factor ζ=0.84 ; f_n=50Hz

B. Modeling Results

The dynamic performance of the proposed voltage control algorithm is first investigated using the inverter small-signal model. Calculations are performed with Matlab/Simulink®. The obtained results are then consolidated through time-domain simulations of an islanded microgrid composed of a single inverter and constant impedance load as illustrated in

Fig. 1a. Table I gives the steady-state conditions of inverter and of microgrid parameters [10].

1) Dominant modes in steady-state: The performance of the proposed control structure is first compared to the voltage control algorithms given in [5]-[8]. The methodology consists of calculating and comparing the eigenvalues of the small-signal models. Three groups of eigenvalues (A, B, C) are clearly identified in the complex plane. The groups presented in red, black and blue are obtained respectively with the approach presented in [6]-[8], in [5], and the approach presented in this paper. The results are shown in Fig. 5a and Fig. 5b.

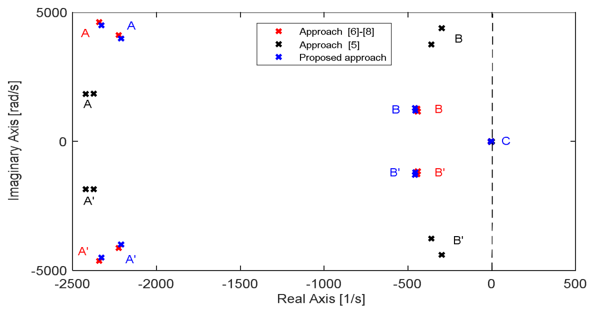

Fig. 5a. Inverter stability in the complex plane from the three voltage control structures. Poles obtained in the steady-state conditions.

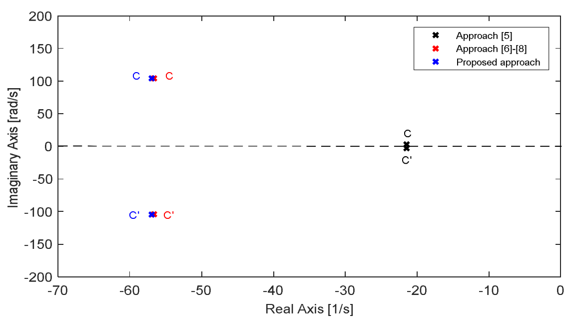

Fig. 5b. Inverter stability in the complex plane from the three voltage control structures. Poles obtained in the steady-state conditions: Zoom on poles C.

a) Eigenvalues A: The results illustrate that the oscillation frequency ω_{osc} of the corresponding poles obtained with our approach (blue A) are close to the poles of approaches in [6]-[8]. The small difference is due to the feedforward loops of $v_{0d(q)}$) that [6]-[8] do not take into account at the output of current control loops of the voltage control algorithms. However, the frequency is higher than that obtained with approach in [5]. This approach (black A) does not consider the decoupling loops of $\omega L_f i_{ld(q)}$ at the output of current control loops in its voltage control structure.

b) Eigenvalues B: These poles show an oscillation frequency higher in [5] (black B) than in [6]-[8] (red B) and our blue B approach. This is because approach [5] does not take into account feedforward loops of $\omega C_f v_{0d(q)}$ and $Fi_{0d(q)}$ at the output of voltage control loops in its control algorithm.

c) Eigenvalues C: The oscillation frequency and damping of the associated poles are very close in the three cases. This is depicted in Fig. 5b. These poles are identified as dominant in the steady-state conditions.

Furthermore, the associated modes to the blue A, red A, black A, and black B eigenvalues can be identified as dominant modes when gain K_{Pc} decreasing (Fig. 6). They are related to the proportional gain of inner current control loops, while black A, blue B and red B eigenvalues are related to the integral gain of internal control loops. The modes associated with these eigenvalues generally influence the global system dynamic performance and stability. The influence of the structure and the parameters of the voltage control algorithm on the system stability can be investigated from the analysis of the movement of the eigenvalues in the stable region.

2) Impact of the parameters of current control loops: Fig. 6 shows the impact of the proportional gain of inner current loops on positioning the dominant poles of the three proposed control algorithms. It shows that decreasing gain strongly affects the stability of eigenvalues in complex plane.

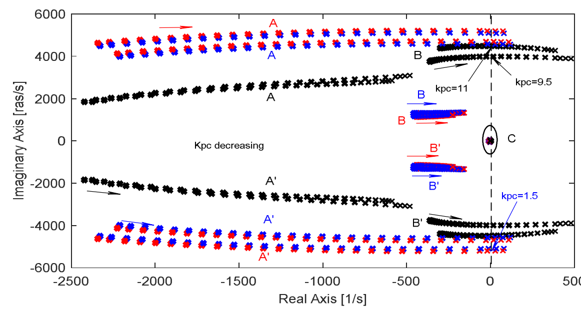

Fig. 6. Impacts of proportional gain K_{Pc} of the current control loops on movement of the dominant poles in the stable region. $0.5 \leq K_{Pc} \leq 27$

a) Eigenvalues A: Blue A, red A and black A poles are moving from left to right in the complex plane. The influence of decoupling loops in the proposed approach (blue A) and in approaches [6]-[8] can be observed from the movement of blue A and red A poles. It is noted that the stability limit results between both control algorithm approaches are close to each other and they are obtained for K_{Pc}=1.5.

b) Eigenvalues B: Firstly, blue B, red B and black B poles are moving from left to right complex plane. Then, the obtained results show that the movement of our approach is close to [6]-[8] but it is very different compared to [5]. This situation is caused by lack of feedforward loops $\omega C_f v_{0d(q)}$ and $Fi_{0d(q)}$ at the output of voltage control loops in [5]. The stability limits (corresponding to a positive real part of a complex eigenvalue) can be reached with all the compared approaches, however for rather different values of the tested parameters.

c) Eigenvalues C: Stability of C poles are close in the three compared approaches.

Furthermore, Fig. 7 depicts the influence of the integral gain of internal current control loops on the movement of poles in the stable region. It is noted that decreasing gain highly affects all the poles without inducing them to instability.

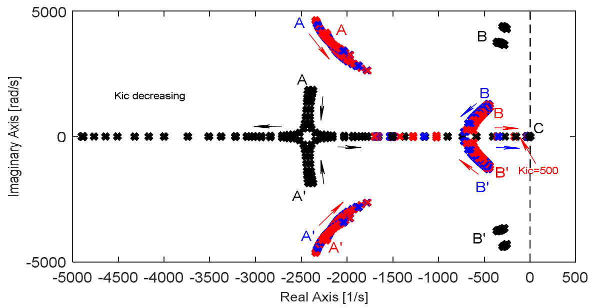

Fig. 7. Impacts of integral gain Kic of the current control loops on movement of the dominant eigenvalues in the stable region. $400 \leq Kic \leq 53e3$

3) Impact of the parameters of voltage control loops: Fig. 8 and Fig. 9 give the obtained eigenvalues in complex plane with increasing K_{Pv} and K_{Iv}, respectively. These results show that the external voltage control loops have a low impact on the movement of poles, therefore on system dynamics and stability. This is observed in Fig. 8 where oscillation frequency ω_{osc} and damping time constant of all eigenvalues groups are less affected by increasing the proportional gain, compared to the effect of the same parameter in the current control loops. The proposed voltage control structure still presents good damping compared to the approach in [5] and close to the [6]-[8] approach. Fig. 9 gives the obtained results with increasing integral gain. It shows that:

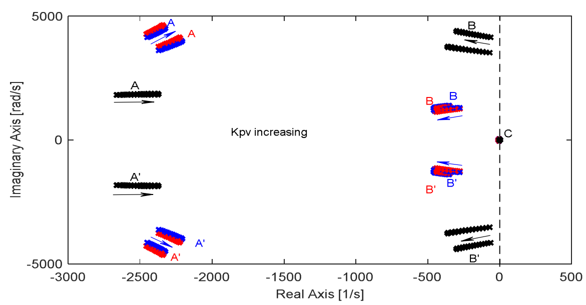

Fig. 8. Impacts of proportional gain K_{Pv} of the external voltage control loops on movement of the dominant eigenvalues in the stable region. $0.03 \leq K_{Pv} \leq 0.14$

a) Eigenvalues A: in our approach (blue A) they move from right to left while the black A eigenvalues move from left to right. This behavior again shows the influence of decoupling terms on the eigenvalues and the dynamics.

b) Eigenvalues B: same behavior compared to the A eigenvalues can be observed in blue B and black B eigenvalues.

4) Optimal controller gains: The obtained modeling results show that the inverter stability is related to the controller gains. Optimal gains are required in order to obtain the optimized eigenvalues in the stable region. To do this, the proposed analytical method in [10] appears as good one, because its computation controller gains depends on the LC filter parameters and the coupling impedance parameters. These factors can be considered as main physical parameters that influence inverter-based islanded microgrid dynamics to the power side. This is demonstrated with the obtained results in Fig. 5a.

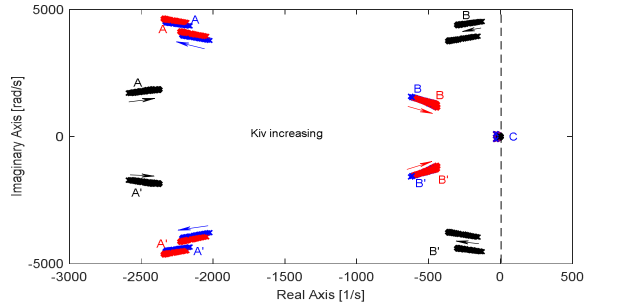

Fig. 9. Impacts of integral gain K_{Iv} of the external voltage control loops on movement of the dominant eigenvalues in the stable region. $39 \leq K_{Iv} \leq 390$

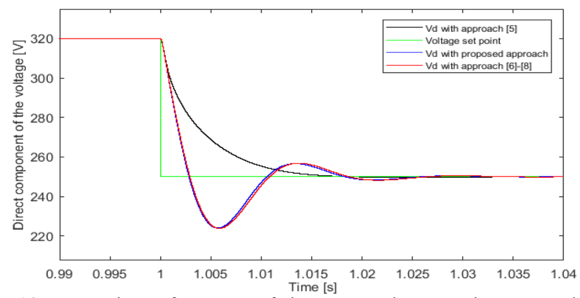

Fig. 10. Dynamic performance of the proposed approach compared to the presented approaches in [5] and [6]-[8]. Direct component of the voltage.

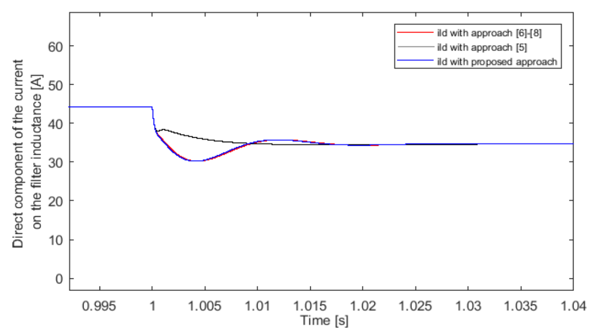

Fig. 11. Dynamic performance of the proposed approach compared to the presented approaches in [5] and [6]-[8]. Direct component of the current on the filter inductance.

C. Time domain simulation

The dynamic performance of the proposed voltage control structure is tested into islanded microgrid model presented in Fig. 1 through time domain simulation (using the Matlab/Simulink Simscape Power Systems environment). The simulation results are given in Fig. 10 to 14. They show that all the state variables stay stable before changing set point of the voltage in the steady-state conditions given in Table I. It is noted that these confirm the results presented in Fig. 5a. However, 20% of set point variation of the direct component of the voltage at the LC filter output after 1s demonstrates that the dynamic responses of the three control schemes are different. Fig. 10 shows the dynamic performance of the direct component of the voltage at the LC filter output. Direct components of the current on LC filter inductance and at the filter output are shown in Fig. 11 and Fig. 12, respectively.

Direct components of voltage signal and current signal at the output of comparators are shown in Fig. 13 and Fig. 14, respectively. It is noted that, regarding dynamic performance results, the effect of the added feedforward and decoupling loops has an important role on the microgrid dynamics and stability. This can have a positive impact on the enhancement of system power quality.

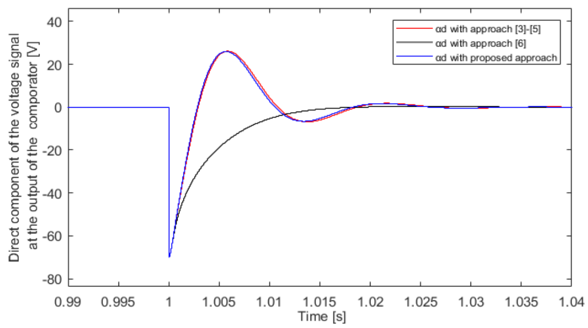

Fig. 13. Dynamic performance of the proposed approach compared to the presented approaches in [5] and [6]-[8]. Direct component of the voltage signal at the output of the comparator.

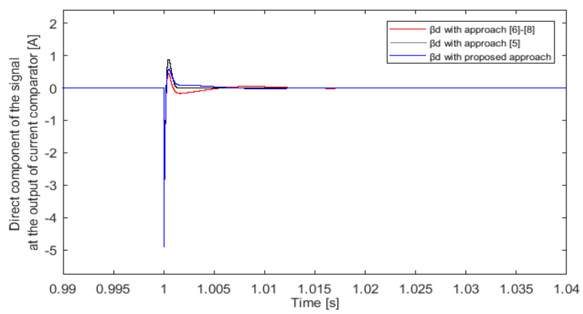

Fig. 14. Dynamic performance of the proposed approach compared to the presented approaches in [5] and [6]-[8]. Direct component of the current signal at the output of the comparator.

IV. CONCLUSION

Small-signal stability of the voltage control structure implemented in three-phase grid-forming voltage source inverter in d-axis and q-axis synchronous reference frame has been investigated. The aim was to identify the influence of feedforward and decoupling loops on inverter dynamics and stability. Firstly, the voltage control structure composed of external voltage and internal current control loops, feedforward and decoupling loops has been proposed. It is obtained from the physical system model of the inverter composed of ideal DC voltage source, LC filter, coupling impedance and local measurements of current and voltage. Beside control loops of current and voltage, additional loops classified as supplementary loops (feedforward and decoupling loops), have been investigated, in order to compensate some effects of current and voltage linked to the physical system model.

Then, the influence of these supplementary loops on inverter dynamics and stability has been investigated through the obtained complete state-space inverter model composed of dynamic sub-models of voltage controller, LC filter and coupling impedance. This was done by analyzing the eigenvalues associated to the dominant modes presented in the stable region. The obtained results are compared to the reported results in existing literature.

This comparison has shown that feedforward loops of $i_{0d(q)}$ and $\omega C_f v_{0d(q)}$, and decoupling loops of $\omega L_f i_{ld(q)}$ enhance the stability limits of the associated eigenvalues to the dominant modes. On the other hand they increase the oscillation frequencies of inverter dynamic response. This can be improved also by adding the feedforward of $v_{0d(q)}$ at the output of current control loops.

Finally, the influence of the additional loops has been assessed to the inverter dynamic performance by considering Simscape Power Systems models of islanded microgrid fed by a single three-phase grid-forming voltage source inverter and constant impedance load. The proposed approach, which consists in adding feedforward and decoupling loops, has been compared to the proposed approaches in the literature [5]-[8]. The obtained simulation results show that the proposed control algorithm presents high performance in terms of oscillation frequency and robustness.

ACKNOWLEDGMENT

The authors would like to acknowledge the financial support provided by the CIA of UCLouvain.

REFERENCES

[1] Md. A. HOSSAIN, H. POTA, W. ISSA, Md. J. HOSSAIN, “Overview of AC microgrid controls with inverter-interfaced generations”, *Energies*, 10 (9), pp. 1300, Aug. 2017.

[2] M. H. Andishgar, E. Gholipour, R.-a. Hooshmand, “An overview of control approaches of inverter-based microgrids in islanding mode of operation”, *Renewable and Sustainable Energy Reviews,* Vol. 80, pp. 1043–1060, 2017.

[3] T.L. Vandoorn, J.D.M. De Kooning, B. Meersman, L.Vandevelde, “Review of primary control strategies for islanded microgrids with power-electronic interfaces”, *Renewable and Sustainable Energy Reviews*, Vol. 19, pp. 613– 628, 2013.

[4] M. Abusara, S. Sharkh, J. M. Guerrero, “Improved Droop Control Strategy for Grid-Connected Inverters”, *Sustainable Energy, Grids and Networks*, Vol. 1, pp. 10-19, Mar. 2015.

[5] J. Rocabert, A. Luna, F. Blaabjerg, P. Rodriguez, “Control of Power Converters in AC Microgrids”, *IEEE Trans. Power Electronics*, Vol. 27, No. 11, pp. 4734-4749, Nov. 2012.

[6] T.C. Green , M. Prodanovic, “ Control of inverter-based micro-grids”, *Electric Power Systems Research,* Vol. 77 , pp. 1204 –1213, 2007.

[7] M. Prodanovic and T. C. Green, “High-Quality Power Generation Through Distributed Control of a Power Park Microgrid”, *IEEE Trans. Industrial Electronics*, Vol. 53, No. 5, pp. 1471-1482, Oct. 2006.

[8] A. Bidram, A. Davoudi, F. Lewis, J. M. Guerrero, “Distributed Cooperative Secondary Control of Microgrids Using Feedback Linearization”, *IEEE Trans. Power Systems*, Vol. 28, No. 3, pp. 3462 – 3470, 2013.

[9] X.-Q. Guo, W. -Y. Wu and H.-R. Gu,“Phase locked loop and synchronization methods for grid-interfaced converters: a review”, *Przegld Elektrotechniczny (Electrical Review)*, ISSN 0033-2097, pp. 182-187, 2011.

[10] G. Wanlongo Ndiwulu, E. De Jaeger, A. Kuti Lusala, “Local stability performance analysis of islanded microgrid based on inner control loops approach”, *CIRED Workshop 2018*, Ljubljana, Jun. 2018.